

Nuclear spin-orbit interaction from chiral pion-nucleon dynamics

N. Kaiser

Physik Department T39, Technische Universität München, D-85747 Garching, Germany

email: nkaiser@physik.tu-muenchen.de

Abstract

Using the two-loop approximation of chiral perturbation theory, we calculate the momentum and density dependent nuclear spin-orbit strength $U_{ls}(p, k_f)$. This quantity is derived from the spin-dependent part of the interaction energy $\Sigma_{spin} = \frac{i}{2} \vec{\sigma} \cdot (\vec{q} \times \vec{p}) U_{ls}(p, k_f)$ of a nucleon scattering off weakly inhomogeneous isospin symmetric nuclear matter. We find that iterated 1π -exchange generates at saturation density, $k_{f0} = 272.7$ MeV, a spin-orbit strength at $p = 0$ of $U_{ls}(0, k_{f0}) \simeq 35$ MeV fm 2 in perfect agreement with the empirical value used in the shell model. This novel spin-orbit strength is neither of relativistic nor of short range origin. The potential V_{ls} underlying the empirical spin-orbit strength $\tilde{U}_{ls} = V_{ls} r_{ls}^2$ becomes a rather weak one, $V_{ls} \simeq 17$ MeV, after the identification $r_{ls} = m_\pi^{-1}$ as suggested by the present calculation. We observe however a strong p -dependence of $U_{ls}(p, k_{f0})$ leading even to a sign change above $p = 200$ MeV. This and other features of the emerging spin-orbit Hamiltonian which go beyond the usual shell model parametrization leave questions about the ultimate relevance of the spin-orbit interaction generated by 2π -exchange for a finite nucleus. We also calculate the complex-valued isovector single-particle potential $U_I(p, k_f) + i W_I(p, k_f)$ in isospin asymmetric nuclear matter proportional to $\tau_3(N - Z)/(N + Z)$. For the real part we find reasonable agreement with empirical values and the imaginary part vanishes at the Fermi-surface $p = k_f$.

PACS: 12.38.Bx, 21.65.+f, 24.10.Cn

Keywords: Effective field theory at finite density, Nuclear spin-orbit interaction, Complex single-particle potential in isospin asymmetric nuclear matter.

1 Introduction and summary

The introduction of the spin-orbit term into the nuclear single-particle Hamiltonian by Haxel, Jensen, Suess and Goeppert-Mayer [1] in 1949 has been most decisive for the success of the nuclear shell model. Only with a very strong and attractive spin-orbit potential one is, for example, able to explain the observed sequence of so-called magic numbers $\{2, 8, 20, 28, 50, 82, 126, \dots\}$. The dynamical origin of the strong nuclear spin-orbit force has not been fully resolved even up to date. The analogy with the spin-orbit interaction in atomic physics gave the hint that it could be a relativistic effect. This idea has lead to the construction of the relativistic (scalar-vector) mean-field model [2]. In this model the spin-independent nuclear potential (of approximate depth -50 MeV) results from an almost complete cancelation of a very strong attraction generated by scalar (σ -meson) exchange and a nearly equally strong repulsion generated by vector (ω -meson) exchange. The corresponding spin-orbit term (obtained by a non-relativistic reduction of the nucleon's Dirac-Hamiltonian) comes out proportional to the coherent sum of the

very large scalar and vector mean-fields. In this sense, the relativistic mean-field model gives a simple and natural explanation of the basic features of the nuclear shell model potential. Refinements of relativistic mean-field models which include additional non-linear couplings of the scalar and vector fields or explicitly density-dependent couplings are nowadays widely and successfully used for nuclear structure calculations [3, 4, 5].

The nuclear spin-orbit potential arises generally as a many-body effect from the underlying spin-orbit term in the (free) nucleon-nucleon scattering amplitude. The calculation of the tree level diagrams with one scalar-meson or one vector-meson exchange between nucleons gives indeed a spin-orbit term in the NN T-matrix proportional to $1/M^2$, with M denoting the nucleon mass. The nuclear spin-orbit potential corresponding to scalar and vector meson exchange is therefore obviously a truly relativistic effect. However, the quadratic reciprocal scaling of the spin-orbit NN-amplitude with the nucleon mass M is not universal, and it changes if one considers the exchange of two mesons between nucleons, i.e. loop diagrams. For example, irreducible two-pion exchange gives rise to a spin-orbit term in the NN T-matrix proportional to $1/M$ (see eqs.(22,23) in ref.[6]) and iterated one-pion exchange produces a spin-orbit term in the NN T-matrix which even scales linearly with the nucleon mass M (see eq.(33) in ref.[6]). It is one of the chief purposes of this paper to investigate in detail the contributions from iterated one-pion exchange to the nuclear spin-orbit interaction. As already mentioned the latter arises from the spin-orbit term in the NN T-matrix as a many-body effect, e.g. in connection with a nuclear matter calculation.

In a recent work [7], we have used chiral perturbation theory for a systematic treatment of the nuclear matter many-body problem. In this calculation the contributions to the energy per particle, $\bar{E}(k_f)$, originate exclusively from one- and two-pion exchange between nucleons and they are ordered in powers of the Fermi momentum k_f (modulo functions of k_f/m_π). It has been demonstrated in ref.[7] that the empirical saturation point and the nuclear matter compressibility $K \simeq 255$ MeV can be well reproduced at order $\mathcal{O}(k_f^5)$ in the chiral expansion with just one single momentum cut-off scale of $\Lambda \simeq 0.65$ GeV which parametrizes all necessary short range dynamics. Most surprisingly, the prediction for the asymmetry energy, $A(k_{f0}) = 33.8$ MeV, is in very good agreement with its empirical value. Furthermore, as a nontrivial fact pure neutron matter is predicted to be unbound and the corresponding equation of state agrees roughly with that of sophisticated many-body calculations for low neutron densities $\rho_n \leq 0.25$ fm $^{-3}$. In a subsequent work [8], the momentum and density dependent (real) single-particle potential $U(p, k_f)$ (i.e. the spin-independent average nuclear mean-field) has been calculated in the same framework. It was found that chiral 1π - and 2π -exchange give rise to a potential depth for a nucleon at the bottom of the Fermi sea of $U(0, k_{f0}) = -53.2$ MeV. This value is in very good agreement with the depth of the empirical optical model potential and the nuclear shell model potential. Nuclear matter at finite temperatures has been investigated in the same framework in ref.[9]. There it was shown that chiral 1π - and 2π -exchange reproduce the first-order liquid-gas phase transition of isospin symmetric nuclear matter with a realistic value $T_c \simeq 19$ MeV of the critical temperature. Our approach to the nuclear matter problem is in many respects different from most other commonly used ones, where one starts from a so-called realistic NN-potential. For example in the relativistic nuclear matter calculation of ref.[10] the S -, P - and D -waves deliver more than 95% of the potential energy per particle. The finding that perturbative chiral pion-nucleon dynamics leads already to good nuclear matter and single particle properties hints at the fact that the detailed NN-interaction is of no more relevance. Fine-tuning of the single cut-off scale Λ to one nuclear matter observable (the binding energy per particle $-\bar{E}(k_{f0})$) is however still necessary in our present approach [7].

It is the purpose of this work to calculate, using the same framework as in ref.[8], the mo-

mentum and density dependent nuclear spin-orbit strength $U_{ls}(p, k_f)$. This quantity is derived from the spin-dependent part of the interaction energy $\Sigma_{spin} = \frac{i}{2} \vec{\sigma} \cdot (\vec{q} \times \vec{p}) U_{ls}(p, k_f)$ of a nucleon scattering off weakly inhomogeneous isospin symmetric nuclear matter. We will present here analytical expressions for the contributions from 1π -exchange and iterated 1π -exchange to the spin-orbit strength $U_{ls}(p, k_f)$. Furthermore, we calculate in isospin asymmetric (homogeneous) nuclear matter the (complex-valued) isovector single-particle potential $U_I(p, k_f) + i W_I(p, k_f)$ accompanied by the isospin double-asymmetry $\tau_3(N - Z)/(N + Z)$. Our results can be summarized as follows:

- i) At nuclear matter saturation density, $k_{f0} = 272.7$ MeV, 1π -exchange and iterated 1π -exchange generate a spin-orbit strength at $p = 0$ of $U_{ls}(0, k_{f0}) = (0.4 + 34.7)$ MeVfm 2 . This result, which is dominated by the contribution of four Hartree-type diagrams, is in perfect agreement with the empirical value of the spin-orbit strength $\tilde{U}_{ls} \simeq 35$ MeVfm 2 [11, 12] used in shell-model calculation of nuclei. The novel spin-orbit strength found here is neither of relativistic nor of short range origin. It is in fact linearly proportional to the nucleon mass M and its inherent range is the pion Compton wavelength $m_\pi^{-1} = 1.46$ fm. The latter feature tempts to an unconventional interpretation of the strong nuclear spin-orbit interaction. The potential V_{ls} underlying the empirical spin-orbit strength $\tilde{U}_{ls} = V_{ls} r_{ls}^2 \simeq 35$ MeVfm 2 becomes a rather weak one, namely $V_{ls} \simeq 17$ MeV, after the identification of the effective range r_{ls} with the pion Compton wavelength, $r_{ls} = m_\pi^{-1}$, as suggested by the present calculation.
- ii) We observe however a strong p -dependence of $U_{ls}(p, k_{f0})$ which leads even to a sign change above $p = 200$ MeV. The calculated spin-orbit strength $U_{ls}(0, k_{f0})$ depends also strongly on the value of the pion mass and it shows a pronounced maximum around $m_\pi \simeq 100$ MeV. A further property of the spin-orbit Hamiltonian emerging from our diagrammatic calculation is that it has (in coordinate space) terms proportional to $\vec{\nabla} f(r)$ as well as terms proportional to $f(r) \vec{\nabla} f(r)$ (with $f(r) = \rho(r)/\rho(0)$ the normalized radial density profile) which get weighted differently at the surface of a finite nucleus. All such features of our calculation which go beyond the usual shell model parametrization of the spin-orbit Hamiltonian leave questions about the ultimate relevance of the spin-orbit interaction generated by 2π -exchange for a finite nucleus. Implementing the present results for $U_{ls}(p, k_f)$ into nuclear structure calculations will clarify the role of the nuclear spin-orbit interaction generated by 2π -exchange.
- iii) The real part of the isovector single-particle potential $U_I(0, k_f)$ generated by chiral 1π - and 2π -exchange has a density dependence very similar to that of the asymmetry energy $A(k_f)$ [7]. At saturation density, $\rho_0 = 0.178$ fm $^{-3}$, we find a repulsive isovector potential of $U_I(0, k_{f0}) = 47$ MeV. This prediction is comparable to the value $U_1 \simeq 33$ MeV used in shell model calculations [11] or the value $U_1 \simeq 40$ MeV deduced from nucleon-nucleus scattering in the framework of the optical model [13]. The momentum dependence of $U_I(p, k_{f0})$ is non-monotonic in the interval $0 \leq p \leq k_{f0}$. One observes a broad maximum at $p = 230$ MeV where the (real) isovector single-particle potential has increased by about 30% to the value 63 MeV. The imaginary part $W_I(p, k_f)$ vanishes (quadratically) at the Fermi-surface ($p = k_f$) in accordance with Luttinger's theorem [14].

2 General considerations about the spin-orbit term

Let us begin with recalling the spin-orbit Hamiltonian of the nuclear shell model [11] which is generally written in the form:

$$\mathcal{H}_{ls} = \tilde{U}_{ls} \frac{\vec{\sigma} \cdot \vec{\ell}}{2r} \frac{df(r)}{dr}, \quad f(r) = \frac{\rho(r)}{\rho(0)}. \quad (1)$$

Here, $\vec{\sigma}$ is the conventional Pauli spin-vector and $\vec{\ell} = \vec{r} \times \vec{p}$ is the orbital angular momentum of a nucleon. $\rho(r)$ denotes the radial density distribution of a nucleus (typically parametrized by a Saxon-Woods function). The empirical value of the nuclear spin-orbit strength is $\tilde{U}_{ls} \simeq 35 \text{ MeVfm}^2$ [11, 12]. This large and positive value of \tilde{U}_{ls} leads to a strongly attractive spin-orbit potential acting mainly at the surface of a nucleus.

We wish to calculate the nuclear spin-orbit strength \tilde{U}_{ls} (or an appropriate generalization of it) in the systematic framework of chiral perturbation theory [7, 8]. The first observation one makes is that the spin-orbit interaction vanishes identically in infinite homogeneous nuclear matter since there is no preferred center in this system in order to define an orbital angular momentum. Therefore one has to generalize the calculation of the single-particle potential in ref.[8] to (at least) weakly inhomogeneous nuclear matter. The relevant quantity in order to extract the nuclear spin-orbit strength is the spin-dependent part of the interaction energy of a nucleon scattering off weakly inhomogeneous isospin symmetric nuclear matter from initial momentum $\vec{p} - \vec{q}/2$ to final momentum $\vec{p} + \vec{q}/2$, which reads:

$$\Sigma_{spin} = \frac{i}{2} \vec{\sigma} \cdot (\vec{q} \times \vec{p}) U_{ls}(p, k_f). \quad (2)$$

The (small) momentum transfer \vec{q} is provided by the Fourier-components of the inhomogeneous nuclear matter distribution. The density form factor $\Phi(\vec{q}) = \int d^3r e^{-i\vec{q} \cdot \vec{r}} f(r)$ plays the role of a probability distribution of these Fourier-components. The form factor $\Phi(\vec{q})$ should be viewed as narrowly peaked function around $\vec{q} = 0$ with its Fourier-transform equal to the (slowly varying) density profile, $f(r) = (2\pi)^{-3} \int d^3q e^{i\vec{q} \cdot \vec{r}} \Phi(\vec{q})$. Using this relationship the spin-orbit Hamiltonian \mathcal{H}_{ls} in eq.(1) becomes equal to the Fourier-transform of the product of the density form factor and the spin-dependent interaction energy: $\mathcal{H}_{ls} = (2\pi)^{-3} \int d^3q e^{i\vec{q} \cdot \vec{r}} \Phi(\vec{q}) \Sigma_{spin}$. Consistent with the assumption of a weakly inhomogeneous nuclear matter distribution we keep in Σ_{spin} only linear terms in \vec{q} corresponding to small spatial density gradients. For practical purposes, this means that after isolating the proportionality factor \vec{q} in an explicit calculation the momentum and density dependent spin-orbit strength $U_{ls}(p, k_f)$ can be finally computed in the limit of homogeneous isospin symmetric nuclear matter (characterized by its Fermi momentum k_f).

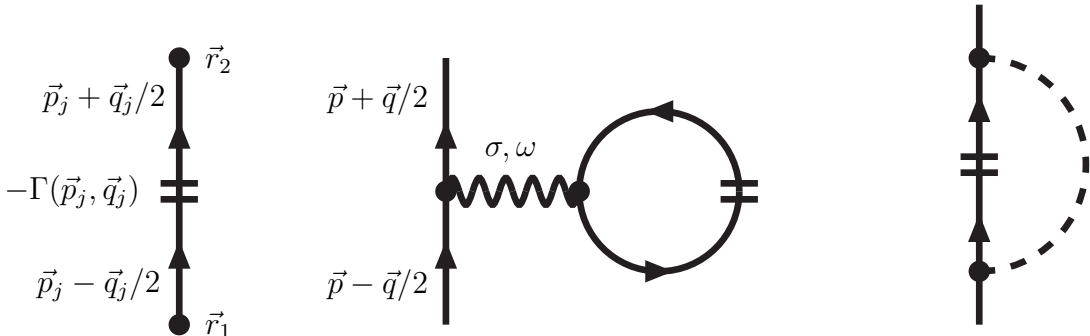


Fig.1: Left: The double line symbolizes the medium insertion for a weakly inhomogeneous many-fermion system $\Gamma(\vec{p}_j, \vec{q}_j)$ defined by eqs.(3,4). Middle: The σ - and ω -exchange Hartree graph. Right: The 1π -exchange Fock graph.

In ref.[8] the calculation of the single-particle potential in homogeneous isospin symmetric nuclear matter has been organized in the number of so-called medium insertions. The latter is a technical notation for the difference between the vacuum and in-medium nucleon propagator (see eq.(3) in ref.[7]). In the case of homogeneous nuclear matter a medium insertion in a self-energy diagram converts effectively a four-dimensional loop integration into an integral over a Fermi-sphere of radius k_f . The medium insertion for a (non-relativistic) many-fermion system is generally constructed from the sum over the occupied energy eigenstates as [15]:

$$\Gamma(\vec{p}_j, \vec{q}_j) = \int d^3 r_1 \int d^3 r_2 \sum_{E \in occ} \psi_E(\vec{r}_2) \psi_E^*(\vec{r}_1) e^{i\vec{p}_j \cdot (\vec{r}_1 - \vec{r}_2)} e^{-\frac{i}{2}\vec{q}_j \cdot (\vec{r}_1 + \vec{r}_2)}. \quad (3)$$

The double line in the left picture of Fig. 1 symbolized this medium insertion together with the assignment of the out- and in-going nucleon momenta $\vec{p}_j \pm \vec{q}_j/2$. The momentum transfer \vec{q}_j is provided by the Fourier-components of the inhomogeneous matter distribution. Semiclassical expansions [15, 16] give for a weakly inhomogeneous and spin-saturated many-fermion system:

$$\Gamma(\vec{p}_j, \vec{q}_j) = \theta(k_f - |\vec{p}_j|) \Phi(\vec{q}_j) \{1 + \mathcal{O}(\vec{q}_j)\}, \quad (4)$$

with $\Phi(\vec{q}_j) \sim \int d^3 p_j \Gamma(\vec{p}_j, \vec{q}_j)$ the density form factor introduced after eq.(2). The subleading $\mathcal{O}(\vec{q}_j)$ term in eq.(4) will in fact never come into play in our diagrammatic calculation of the spin-dependent interaction energy Σ_{spin} to linear order in \vec{q} .

As a first check on this formalism we evaluate the σ - and ω -exchange Hartree diagram in Fig. 1. We perform the non-relativistic $1/M$ -expansion of the scalar/vector interaction vertex sandwiched between Dirac-spinors for the out- and in-going nucleon (of momentum $\vec{p} \pm \vec{q}/2$) until we obtain the spin-orbit like term $i\vec{\sigma} \cdot (\vec{q} \times \vec{p})/4M^2$. After that we can take the limit of homogeneous nuclear matter and perform the remaining integral over a Fermi-sphere of radius k_f which brings one factor of density ρ . Putting all pieces together we reproduce the familiar result:

$$U_{ls}^{(\sigma\omega)}(p, k_f) = \frac{\rho}{2M^2} \left(\frac{g_{\sigma N}^2}{m_\sigma^2} + \frac{g_{\omega N}^2}{m_\omega^2} \right), \quad \rho = \frac{2k_f^3}{3\pi^2}, \quad (5)$$

of the relativistic mean-field model [2, 3]. The contribution of the analogous σ - and ω -exchange Fock diagrams to the nuclear spin-orbit strength can also be easily calculated with the help of the formalism outlined above. We obtain from these Fock diagrams $1/4$ of the σ -exchange contribution and $3/4$ of the ω -exchange contribution written in eq.(5). In this work our main interest is focussed on the nuclear spin-orbit interaction generated by chiral one- and two-pion exchange.

3 Diagrammatic calculation of the spin-orbit strength

In this section we present analytical results for the nuclear spin-orbit strength $U_{ls}(p, k_f)$ as given by chiral one- and two-pion exchange. We start with the 1π -exchange Fock graph (last diagram in Fig. 1). In the static approximation the product of πN -interaction vertices $\vec{\sigma} \cdot (\vec{p} - \vec{p}_1) \vec{\sigma} \cdot (\vec{p} - \vec{p}_1) = (\vec{p} - \vec{p}_1)^2$ is spin-independent. A non-vanishing nuclear spin-orbit strength comes therefore only as a relativistic $1/M^2$ -correction. Isolating the $i\vec{\sigma} \times \vec{q}$ factor from the product of fully relativistic pseudovector πN -interaction vertices, performing the $1/M$ -expansion, and integrating finally over a Fermi-sphere of radius k_f , we get from the 1π -exchange Fock diagram:

$$U_{ls}^{(1\pi)}(p, k_f) = \frac{g_A^2 m_\pi^3}{(8\pi f_\pi M x)^2} \left\{ u^5 - ux^4 - \frac{4}{3}u^3 x^2 + \frac{u}{2}(u^2 + 5x^2 - 1) \right\}$$

$$\begin{aligned}
& -4x^2 \left[\arctan(u+x) + \arctan(u-x) \right] \\
& + \left[(x^2 - u^2)^3 - \frac{3}{2}(x^2 - u^2)^2 + 6x^2 + \frac{1}{2} \right] L(x, u) \Big\}. \tag{6}
\end{aligned}$$

Here, we have introduced the dimensionless variables $x = p/m_\pi$ and $u = k_f/m_\pi$ and the auxiliary function

$$L(x, u) = \frac{1}{4x} \ln \frac{1 + (u+x)^2}{1 + (u-x)^2}. \tag{7}$$

For the readers convenience we will present the spin-orbit strength at $p = 0$ of each individual diagram in a separate formula, since in most cases the limit $x \rightarrow 0$ is quite non-trivial. For the 1π -exchange Fock diagram we find the simple expression

$$U_{ls}^{(1\pi)}(0, k_f) = \frac{g_A^2 m_\pi^3}{(4\pi f_\pi M)^2} \left\{ \frac{u^3}{3} + u + \frac{u}{1+u^2} - 2 \arctan u \right\}, \tag{8}$$

which gives numerically at saturation density $k_{f0} = 272.7$ MeV only about 1.1% of the empirical value $\tilde{U}_{ls} \simeq 35$ MeVfm 2 .

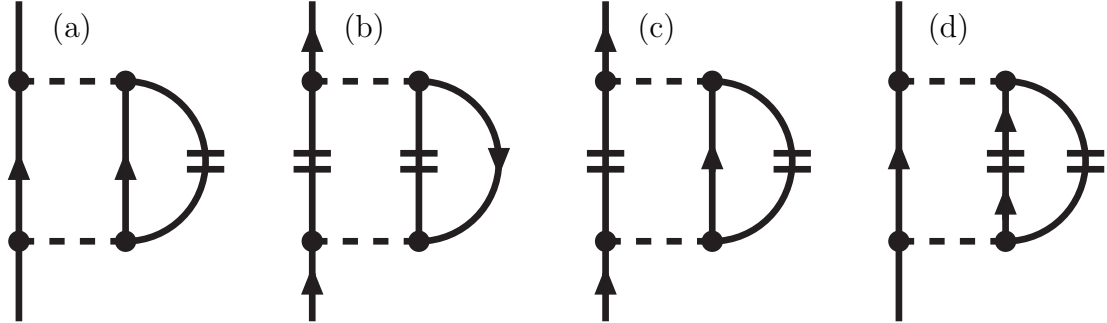


Fig.2: The iterated 1π -exchange Hartree graphs. Their isospin factor in symmetric nuclear matter is 6.

Next, we come to the evaluation of the four Hartree diagrams of iterated one-pion exchange shown in Fig. 2. We start with the left graph with one medium insertion, labeled (a). The relevant $i \vec{\sigma} \times \vec{q}$ prefactor can be isolated already in the first step of the calculation from the product of πN -interaction vertices $\vec{\sigma} \cdot (\vec{l} - \vec{q}/2) \vec{\sigma} \cdot (\vec{l} + \vec{q}/2)$ at the open nucleon line. For all remaining parts of the diagram one can then take the limit of homogeneous nuclear matter (i.e. $\vec{q} = 0$). Using the analytical results given in section 4.3 of ref.[6] for the inner d^3l -loop integral we can even perform the integral over a Fermi-sphere of radius k_f . Altogether, we find the following closed form expression for the spin-orbit strength generated by the Hartree diagram (a):

$$\begin{aligned}
U_{ls}^{(a)}(p, k_f) = & \frac{2g_A^4 M m_\pi^2}{(8\pi x)^3 f_\pi^4} \left\{ 16(u^3 + x^3) \arctan(u+x) + 16(x^3 - u^3) \arctan(u-x) \right. \\
& \left. + ux(7 - 9u^2 - 9x^2) + [9(u^2 - x^2)^2 - 30u^2 - 30x^2 - 7] x L(x, u) \right\}. \tag{9}
\end{aligned}$$

At zero nucleon momentum ($p = 0$) this simplifies to

$$U_{ls}^{(a)}(0, k_f) = \frac{g_A^4 M m_\pi^2}{32\pi^3 f_\pi^4} \left\{ 4 \arctan u - 3u - \frac{u}{1+u^2} \right\}. \tag{10}$$

Note also that $U_{ls}^{(a)}(p, k_f)$ in eq.(9) originates from the real part of the iterated 1π -exchange spin-orbit NN-amplitude (eq.(33) in ref.[6]) evaluated in forward direction and integrated over a Fermi-sphere of radius k_f .

We continue with the calculation of the Hartree diagrams with two medium insertions, labeled (b), (c) and (d) in Fig. 2. In these diagrams, a (small) momentum transfer $\vec{q}_{1,2}$ with $\vec{q} = \vec{q}_1 + \vec{q}_2$ occurs at each medium insertion. The important prefactors $i\vec{\sigma} \times \vec{q}_j$ can again be isolated in the first step of the calculation from the product of πN -interaction vertices at the open nucleon line. After that the vectors \vec{q}_j can be set to zero in all remaining components of these diagrams. When Fourier-transformed with the density form factors to coordinate space each such momentum transfer \vec{q}_j , ($j = 1, 2$) leads to the expression: $(2\pi)^{-6} \int d^3q \int d^3q_j e^{i\vec{q} \cdot \vec{r}} i\vec{q}_j \Phi(\vec{q}_j) \Phi(\vec{q} - \vec{q}_j) = f(r) \vec{\nabla} f(r)$, with $f(r)$ the density profile of weakly inhomogeneous nuclear matter. Consistent with the assumption of a weakly inhomogeneous nuclear matter (i.e. keeping only linear terms in small spatial gradients) we can make the replacement: $f(r) \vec{\nabla} f(r) \rightarrow \vec{\nabla} f(r)$. We will come back to this point in the next section when discussing the results for the spin-orbit strength $U_{ls}(p, k_f)$ as well as their relevance for a finite nucleus. The essential conclusion from the previous considerations is that for the calculation of Σ_{spin} in weakly inhomogeneous nuclear matter each momentum transfer \vec{q}_j can be identified with \vec{q} . With the help of this rule and certain techniques to reduce six-dimensional principal value integrals over the product of two Fermi-spheres of radius k_f , we end up with the following result for the Hartree diagram (b):

$$U_{ls}^{(b)}(p, k_f) = \frac{6g_A^4 M m_\pi^2}{(4\pi f_\pi)^4} \int_{-1}^1 dy \frac{y}{x} \left[2uxy + (u^2 - x^2 y^2) \ln \frac{u+xy}{u-xy} \right] \left[\frac{3s+2s^3}{1+s^2} - 3 \arctan s \right], \quad (11)$$

with the auxiliary function $s = xy + \sqrt{u^2 - x^2 + x^2 y^2}$. Throughout this work the momentum p is restricted to the interval $0 \leq p \leq k_f$. At zero nucleon momentum ($p = 0$) eq.(11) simplifies to

$$U_{ls}^{(b)}(0, k_f) = \frac{g_A^4 M m_\pi^2}{(2\pi f_\pi)^4} \left\{ 2u^2 + \frac{u^2}{1+u^2} - 3u \arctan u \right\}. \quad (12)$$

Similarly, we find for the Hartree diagram (c):

$$U_{ls}^{(c)}(p, k_f) = \frac{12g_A^4 M m_\pi^2}{(4\pi f_\pi)^4} \int_{-1}^1 dy \int_{-xy}^{s-xy} d\xi \frac{y(xy+\xi)^4}{x[1+(xy+\xi)^2]^2} \left[2u\xi + (u^2 - \xi^2) \ln \frac{u+\xi}{u-\xi} \right], \quad (13)$$

$$\begin{aligned} U_{ls}^{(c)}(0, k_f) = & \frac{g_A^4 M m_\pi^2}{(2\pi f_\pi)^4} \int_0^u d\xi \frac{\xi^4}{(1+\xi^2)^3} \left\{ -u(7+3\xi^2) \right. \\ & \left. + (5u+7\xi+u\xi^2+3\xi^3) \left[1 + \frac{u-\xi}{2u} \ln \frac{u+\xi}{u-\xi} \right] \right\}, \end{aligned} \quad (14)$$

and for the Hartree diagram (d):

$$U_{ls}^{(d)}(p, k_f) = \frac{3g_A^4 M m_\pi^2}{(2\pi f_\pi)^4} \int_0^u d\xi \frac{\xi^2}{x^3} \int_{-1}^1 dy \left[\frac{\xi y}{2} \ln \frac{|x+\xi y|}{|x-\xi y|} - x \right] \left[\frac{3\sigma+2\sigma^3}{1+\sigma^2} - 3 \arctan \sigma \right], \quad (15)$$

with the auxiliary function $\sigma = \xi y + \sqrt{u^2 - \xi^2 + \xi^2 y^2}$. The limit $x \rightarrow 0$ of eq.(15) is quite non-trivial since it requires a careful treatment of the singular function $\text{Re}(y+i0)^{-2}$. The following representation is manifestly free of singularities,

$$\begin{aligned} U_{ls}^{(d)}(0, k_f) = & \frac{g_A^4 M m_\pi^2}{(2\pi f_\pi)^4} \int_0^u d\xi \int_{-1}^1 \frac{dy}{y^2} \left\{ \frac{3\sigma+2\sigma^3}{1+\sigma^2} - 3 \arctan \sigma - \frac{2\xi y(u^2 - \xi^2)^2}{(1+u^2 - \xi^2)^2} \right. \\ & \left. + (1+y^2) \left[3 \arctan \sqrt{u^2 - \xi^2} - \frac{3+2u^2-2\xi^2}{1+u^2-\xi^2} \sqrt{u^2 - \xi^2} \right] \right\}. \end{aligned} \quad (16)$$

Note also the similarity of the expressions eqs.(11,13,15) with the three-body single-particle potential given in eq.(11) of ref.[8].

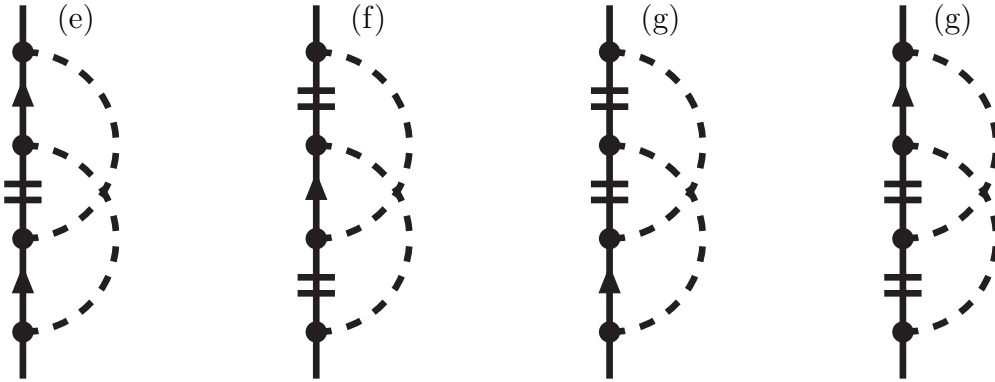


Fig.3: The iterated 1π -exchange Fock graphs. Their isospin factor in symmetric nuclear matter is -3 .

Next, we come to the evaluation of the four iterated 1π -exchange Fock diagrams shown in Fig.3. We start with diagram (e) with one medium insertion. Let us first consider the πN -interaction vertices. The spin-dependent part of the matrix-product $\vec{\sigma} \cdot \vec{a} \vec{\sigma} \cdot \vec{b} \vec{\sigma} \cdot \vec{a} \vec{\sigma} \cdot \vec{b}$ is $2i \vec{a} \cdot \vec{b} \vec{\sigma} \cdot (\vec{a} \times \vec{b})$. In the case of graph (e) one makes the assignment: $\vec{a} = \vec{l} + \vec{Q}$ and $\vec{b} = \vec{l}$, with \vec{l} the loop momentum and $\vec{Q} = \vec{p}_1 - \vec{p}$, where \vec{p} belongs to the external nucleon line and \vec{p}_1 to the internal nucleon line carrying the medium insertion. The important proportionality factor \vec{q} is now not produced by the πN -interaction vertices as it was the case for the Hartree diagrams in Fig.2. In order to isolate the factor \vec{q} we combine the previously mentioned $\vec{a} \cdot \vec{b}$ term with the nucleon energy denominator (which in the actual calculation results from the dl_0 -loop integration) and employ the identity: $\vec{l} \cdot (\vec{l} + \vec{Q}) [\vec{l} \cdot (\vec{l} + \vec{Q} + \vec{q})]^{-1} = 1 - \vec{l} \cdot \vec{q} [\vec{l} \cdot (\vec{l} + \vec{Q} + \vec{q})]^{-1}$. The term coming along with 1 in this decomposition finally loop-integrates to zero. From the second term one can now easily isolate the factor \vec{q} and take the limit to homogeneous nuclear matter of all remaining factors of the diagram. Putting all pieces together we end up with the following representation for the nuclear spin-orbit strength generated by the iterated 1π -exchange Fock diagram (e):

$$U_{ls}^{(e)}(p, k_f) = \frac{3g_A^4 M m_\pi^2}{(8\pi x)^3 f_\pi^4} \left\{ ux(u^2 + x^2) - \frac{1}{2}(u^2 - x^2)^2 \ln \frac{u+x}{u-x} \right. \\ \left. + \int_{(u-x)/2}^{(u+x)/2} d\xi \frac{[u^2 - (2\xi + x)^2][u^2 - (2\xi - x)^2]}{4\xi^2(1 + 2\xi^2)} \right. \\ \left. \times [(1 + 4\xi^2) \arctan 2\xi - 4\xi^2(1 + \xi^2) \arctan \xi] \right\}, \quad (17)$$

$$U_{ls}^{(e)}(0, k_f) = \frac{g_A^4 M m_\pi^2}{(4\pi)^3 f_\pi^4} \left\{ u + \frac{1}{2+u^2} \left[\frac{u^2}{2} (4+u^2) \arctan \frac{u}{2} - 2(1+u^2) \arctan u \right] \right\}. \quad (18)$$

Note also that $U_{ls}^{(e)}(p, k_f)$ in eq.(17) originates from the real part of the iterated 1π -exchange spin-orbit NN-amplitude (eq.(33) in ref.[6]) evaluated in backward direction and integrated over a Fermi-sphere of radius k_f .

We continue with the computation of the Fock diagrams with two medium insertion, labeled (f) and (g) in Fig.3. Diagram (f) with a symmetrical arrangement of the two medium insertions

leads to the following contribution to the nuclear spin-orbit strength:

$$\begin{aligned}
U_{ls}^{(f)}(p, k_f) = & \frac{3g_A^4 M m_\pi^2}{(4\pi f_\pi)^4} \left\{ \frac{1}{4x^4} \left[(x^2(4u^2 - 3x^2) - (1+u^2)^2) L(x, u) \right. \right. \\
& + u(1+u^2 + 3x^2) - 2x^2 (\arctan(u+x) + \arctan(u-x)) \Big] \\
& \times \left[u(1+u^2 + x^2) - [1+(u+x)^2][1+(u-x)^2] L(x, u) \right] \\
& \left. + \int_{-1}^1 dy \int_{-1}^1 dz \frac{y|z| \theta(y^2 + z^2 - 1)}{x|y|\sqrt{y^2 + z^2 - 1}} [\ln(1+s^2) - s^2] [t - \arctan t] \right\}, \quad (19)
\end{aligned}$$

with the auxiliary function $t = xz + \sqrt{u^2 - x^2 + x^2 z^2}$. At zero nucleon momentum ($p = 0$) the lengthy expression eq.(19) simplifies drastically to

$$U_{ls}^{(f)}(0, k_f) = \frac{g_A^4 M m_\pi^2}{(2\pi f_\pi)^4} \frac{u^6}{3(1+u^2)^2}. \quad (20)$$

Note the leading ρ^2 -behavior of the expressions in eqs.(12,20) derived from diagrams with two medium insertions. The results eqs.(8,10,18) belonging to diagrams with one medium insertion, on the other hand, show a leading linear dependence on the density $\rho \sim u^3$.

Finally, we have to evaluate the last two topologically distinct Fock diagrams in Fig. 3. Since they contribute equally to the nuclear spin-orbit strength we have given both diagrams the same label (g). In order to avoid very lengthy formulas we split their contribution to $U_{ls}(p, k_f)$ into a "factorizable" (g') and a "non-factorizable" part (g''). Technically these two pieces are distinguished by the feature whether the nucleon propagator in the denominator can be canceled by terms from the product of πN -interaction vertices in the numerator, or not. We find from the iterated 1π -exchange Fock diagrams (g) with two medium insertions the following "factorizable" contribution to the nuclear spin-orbit strength:

$$\begin{aligned}
U_{ls}^{(g')}(p, k_f) = & \frac{3g_A^4 M m_\pi^2}{(4\pi f_\pi)^4 x^3} \int_0^u d\xi \left\{ \frac{3ux}{2\xi^2} (1+u^2)(1+x^2) - \frac{ux}{2} (12\xi^2 + 1 + x^2) \right. \\
& + 4\xi^2 [\arctan(u+\xi) + \arctan(u-\xi)] [x + (x^2 - 1 - \xi^2) L(\xi, x)] \\
& + \left[\frac{3\xi^4}{2} (4u^2 + 5x^2 - 3) + \frac{\xi^2}{2} (5 + 10u^2 - 4x^2 - 14u^2 x^2 - x^4) - 6\xi^6 - u^2 x^4 \right. \\
& + \frac{1}{2} (5 + 3u^4 + 3x^2 - u^4 x^2) + 2u^2 + x^4 - 3u^2 x^2 + \frac{3}{2\xi^2} (1+u^2)^2 (1+x^2)^2 \Big] \\
& \times L(\xi, x) L(\xi, u) + \left[6\xi^4 + \frac{\xi^2}{2} (x^2 - 12u^2 - 3) + (1+x^2)(u^2 - 1) \right. \\
& - \frac{3}{2\xi^2} (1+x^2)(1+u^2)^2 \Big] x L(\xi, u) + \left[6\xi^4 + \frac{\xi^2}{2} (13 - 15x^2) \right. \\
& \left. \left. + \frac{1}{2} (x^4 + u^2 x^2 + 3x^2 - 3u^2 - 2) - \frac{3}{2\xi^2} (1+x^2)^2 (1+u^2) \right] u L(\xi, x) \right\}, \quad (21)
\end{aligned}$$

which turns at zero nucleon momentum ($p = 0$) into the form:

$$\begin{aligned}
U_{ls}^{(g')}(0, k_f) = & \frac{2g_A^4 M m_\pi^2}{(4\pi f_\pi)^4} \int_0^u d\xi \frac{\xi^2}{(1+\xi^2)^2} \left\{ u(3u^2 - 9\xi^2 - 17) + 4(3 + \xi^2) [\arctan(u+\xi) \right. \\
& \left. + \arctan(u-\xi)] + (9\xi^4 - 6u^2 \xi^2 + 18\xi^2 - 3u^4 - 26u^2 - 7) L(\xi, u) \right\}. \quad (22)
\end{aligned}$$

The analytical evaluation of the "non-factorizable" parts from diagrams (g) terminates with two non-elementary integrations and we find the following representation for their contribution to the nuclear spin-orbit strength:

$$\begin{aligned}
U_{ls}^{(g'')}(p, k_f) = & \frac{3g_A^4 M m_\pi^2}{(4\pi f_\pi)^4} \int_0^u d\xi \frac{\xi^2}{x^3} \int_{-1}^1 dy \left\{ 8[\sigma - \arctan \sigma] [x - L(\xi, x)] \right. \\
& + \left[\frac{1}{2} \ln(1 + \sigma^2) + 4\xi y \arctan \sigma + 2u^2 - 2\xi^2 - \frac{5}{2}\sigma^2 \right] \ln \frac{|x + \xi y|}{|x - \xi y|} \\
& + \left[4\xi y \arctan \sigma + \frac{1}{2}(1 + \xi^2 - x^2) \ln(1 + \sigma^2) + 2u^2 - 2\xi^2 \right. \\
& \left. \left. + \frac{\sigma^2}{2}(x^2 - 5 - \xi^2) \right] \frac{1}{R} \ln \frac{|xR + (x^2 - 1 - \xi^2)\xi y|}{|xR + (1 + \xi^2 - x^2)\xi y|} \right\}, \quad (23)
\end{aligned}$$

with the auxiliary function $R = \sqrt{(1 + x^2 - \xi^2)^2 + 4\xi^2(1 - y^2)}$. At zero nucleon momentum ($p = 0$) eq.(23) turns into the (singularity free) form:

$$\begin{aligned}
U_{ls}^{(g'')}(0, k_f) = & \frac{4g_A^4 M m_\pi^2}{(4\pi f_\pi)^4} \int_0^u d\xi \frac{\xi}{(1 + \xi^2)^2} \int_{-1}^1 \frac{dy}{y^2} \left\{ 2\xi(1 + \xi^2 - 2y^2) [\arctan \sigma - \sigma] \right. \\
& + y \left[\ln(1 + \sigma^2) - \ln(1 + u^2 - \xi^2) - 2\xi y \sigma + \frac{2\xi^2(1 + \xi^2)(u^2 - \xi^2)}{1 + u^2 - \xi^2} \right] \\
& \left. + 2\xi(1 + \xi^2)(1 + y^2) [\sqrt{u^2 - \xi^2} - \arctan \sqrt{u^2 - \xi^2}] \right\}. \quad (24)
\end{aligned}$$

Note again the similarity of the expressions in eqs.(19,21,23) with the three-body potential given in eq.(13) of ref.[8]. We also like to emphasize that the techniques used to reduce six-dimensional principal value integrals over the product of two Fermi-spheres of radius k_f to at most double integrals have been checked rigorously in ref.[8] via the Hugenholtz-van-Hove theorem.

Let us end this section with power counting considerations for the spin-dependent interaction energy Σ_{spin} . Counting the quantities \vec{p} , \vec{q} , k_f and m_π collectively as small momenta, we deduce that the relativistic $1/M^2$ -correction from the 1π -exchange Fock graph is of fifth order, while all contributions from iterated 1π -exchange are of fourth order in small momenta. Irreducible 2π -exchange gives also rise to a fifth order contribution to the (real part of the) single-particle potential (see eq.(16) in ref.[8]). To the spin-orbit NN-amplitude irreducible 2π -exchange contributes as a (higher-order) relativistic $1/M$ -correction (see eqs.(22,23) in ref.[6]) and it will therefore enter Σ_{spin} at sixth order in small momenta. We have also checked that the relativistic $1/M$ -corrections to iterated 1π -exchange start to contribute to Σ_{spin} first at sixth order in small momenta. From all that we can conclude that the present calculation of the nuclear spin-orbit strength $U_{ls}(p, k_f)$ is complete up-to-and-including third order in small momenta. Strictly speaking, this counting argument applies only to the long-range effects induced by chiral 1π - and 2π -exchange since it does not cover the possible short-range contribution, $U_{ls}^{(short)}(p, k_f) = C_{ls} \rho$, which is of course also of third order in small momenta. From this point of view the $\sigma\omega$ -exchange term eq.(5) (together with the Fock contributions) provides a model for the a priori undetermined low-energy constant C_{ls} . In order to learn about the convergence of the chiral expansion of the nuclear spin-orbit strength $U_{ls}(p, k_f)$ one should calculate the contributions from irreducible 2π -exchange of fourth order in small momenta. Work along this line is in progress. Furthermore, we note that spin-orbit strength generated by the three-body force diagrams in Fig. 2 of ref.[17] is (formally) of higher order in small momenta. These should also be evaluated with the formalism introduced in section 2.

Diagram	1 π -Fock	(a)	(b)	(c)	(d)	(e)	(f)	(g')	(g'')
$U_{ls}(0, k_{f0})$	0.40	-52.96	37.35	41.11	12.57	30.33	14.69	-44.50	-3.85
$U_{ls}(k_{f0}, k_{f0})$	-0.28	-40.05	31.63	13.95	-35.35	25.63	4.35	-29.05	8.04

Table 1: Contributions of individual diagrams to the nuclear spin-orbit strength $U_{ls}(p, k_{f0})$ at $p = 0$ and at $p = k_{f0} = 272.7$ MeV. The units are MeVfm².

3.1 Results

For the numerical evaluation of the nuclear spin-orbit strength $U_{ls}(p, k_f)$ we use consistently the same parameters as in our previous works [7, 8]. We choose the value $g_A = 1.3$ for the nucleon axial vector coupling constant. The weak pion decay constant has the value $f_\pi = 92.4$ MeV and $M = 939$ MeV and $m_\pi = 135$ MeV are the masses of the nucleon and the (neutral) pion, respectively.

In the second row of Table 1, we present numerical values for the contributions of individual diagrams to the spin-orbit strength $U_{ls}(0, k_{f0})$ at nuclear matter saturation density $k_{f0} = 272.7$ MeV. As expected the relativistic $1/M^2$ -correction from the 1 π -exchange Fock graph is a very small 1.1% effect. The contributions of individual iterated 1 π -exchange diagrams are surprisingly large. In several cases they even exceed the empirical value $\tilde{U}_{ls} \simeq 35$ MeVfm² in magnitude and moreover they are of alternating signs. The basic reason for these large values is the large scale enhancement factor M (the nucleon mass) entering the iterated 1 π -exchange. The proportionality factor M stems from the energy denominator of such second-order diagrams which is a difference of small nucleon kinetic energies. Adding up the entries in the second row of Table 1 one gets $U_{ls}(0, k_{f0}) = 35.1$ MeVfm², which is in perfect agreement with the empirical value of the nuclear spin-orbit strength $\tilde{U}_{ls} \simeq 35$ MeVfm² [11, 12]. The predicted total sum is dominated by the contribution $U_{ls}^{(H)}(0, k_{f0}) = 38.1$ MeVfm² of the four Hartree diagrams (a), (b), (c) and (d) (see Fig. 2). Interestingly, the same feature, namely the numerical suppression of the iterated 1 π -exchange Fock diagrams against the Hartree diagrams, holds also for the (spin-independent) nuclear mean-field $U(p, k_f)$ studied in ref.[8]. The novel spin-orbit strength generated (almost completely) by iterated 1 π -exchange is neither of relativistic nor of short range origin. It is in fact linearly proportional to the nucleon mass M and its inherent range is the pion Compton wavelength $m_\pi^{-1} = 1.46$ fm. The latter feature tempts to an unconventional interpretation of the strong nuclear spin-orbit interaction. The potential V_{ls} underlying the empirical spin-orbit strength $\tilde{U}_{ls} = V_{ls} r_{ls}^2 \simeq 35$ MeVfm² becomes a rather weak one, namely $V_{ls} \simeq 17$ MeV, after the identification of the effective range r_{ls} with the pion Compton wavelength, $r_{ls} = m_\pi^{-1} = 1.46$ fm, as suggested by the present calculation.

As a side remark we consider $U_{ls}(0, k_f)$ in the chiral limit $m_\pi = 0$. In that case all occurring integrals can be performed analytically and we find the following simple expression:

$$U_{ls}(0, k_f)_{|m_\pi=0} = \frac{g_A^4 M k_f^2}{(4\pi f_\pi)^4} \left(\frac{4}{3} - \frac{\pi^2}{2} \right) + \frac{g_A^2 k_f^3}{3(4\pi f_\pi M)^2}, \quad (25)$$

which gives at $k_{f0} = 272.7$ MeV the negative value -15.0 MeVfm².

In Fig. 4, we show the pion mass dependence of the nuclear spin-orbit strength $U_{ls}(0, k_{f0})$ at nuclear matter saturation density (and zero nucleon momentum). One observes a sign change and a pronounced maximum at $m_\pi \simeq 100$ MeV.

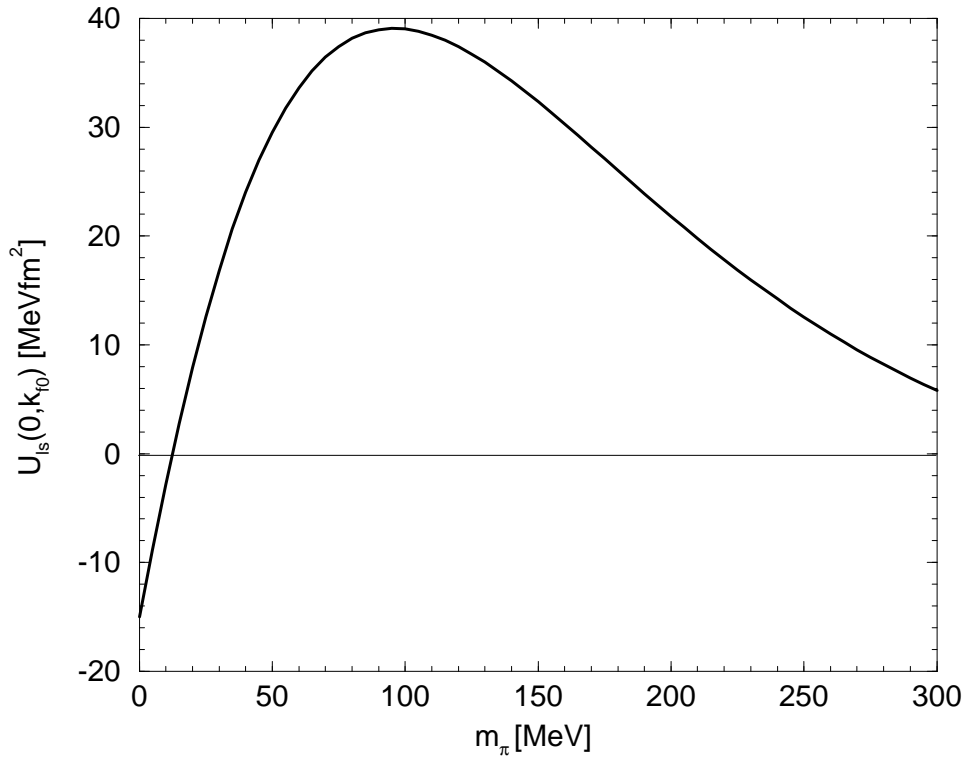


Fig. 4: The pion mass dependence of the nuclear spin-orbit strength $U_{ls}(0, k_{f0})$ at saturation density $k_{f0} = 272.7$ MeV.

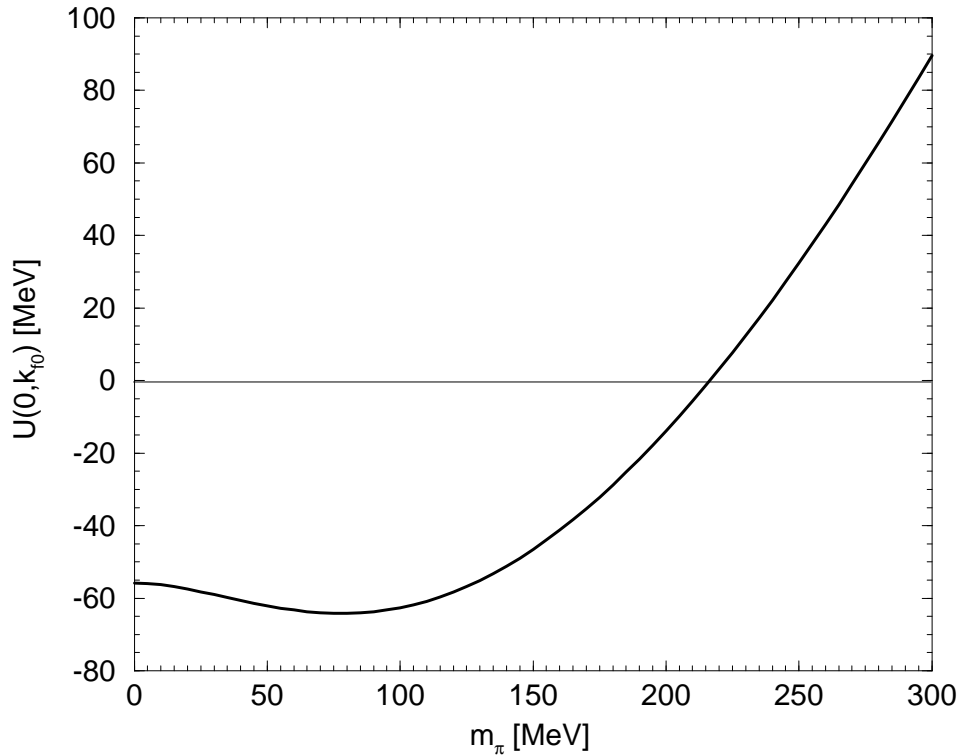


Fig. 5: The pion mass dependence of the depth of the spin-independent single-particle potential $U(0, k_{f0})$ [8] at saturation density $k_{f0} = 272.7$ MeV.

This strong m_π -dependence of $U_{ls}(0, k_{f0})$ has its origin in the alternating signs of the large contributions from individual diagrams as well as their own specific m_π -dependence. For comparison, we show in Fig. 5 the pion mass dependence of the depth of the (real) single-particle potential $U(0, k_{f0})$ calculated in ref.[8]. One observes a weak variation of the potential depth $U(0, k_{f0})$ by at most 10% if m_π runs from zero (chiral limit) to the physical value $m_\pi = 135$ MeV. With increasing pion mass the attractive nuclear mean-field generated by chiral 2π -exchange gets however soon lost and it turns into repulsion above $m_\pi \simeq 215$ MeV.

In Fig. 6, we show by the full line the dependence of the calculated nuclear spin-orbit strength $U_{ls}(0, k_f)$ on the nucleon density $\rho = 2k_f^3/3\pi^2$. One observes in the region $\rho \leq 0.4 \text{ fm}^{-3}$ an approximate linear growth of $U_{ls}(0, k_f)$ with the density as it is, for example, known from σ - and ω -exchange (see eq.(5)).

In a finite nucleus the spin-orbit force acts mainly on the surface where the density gradients are largest and the density has dropped to about half of the central density. The replacement $f(r) \vec{\nabla} f(r) \rightarrow \frac{1}{2} \vec{\nabla} f(r)$ (instead of $f(r) \vec{\nabla} f(r) \rightarrow \vec{\nabla} f(r)$ valid for weakly inhomogeneous nuclear matter) describes then more realistically the situation for a finite nucleus. The dashed line in Fig. 6 shows the spin-orbit strength which results if the contributions from the diagrams with two medium insertion (b), (c), (d), (f) and (g) are weighted with a factor 1/2. This different weighting leads to a substantial reduction of the total spin-orbit strength such that only about 18% of the empirical value $\tilde{U}_{ls} \simeq 35 \text{ MeV fm}^2$ are left at nuclear matter saturation density $\rho_0 = 0.178 \text{ fm}^{-3}$.

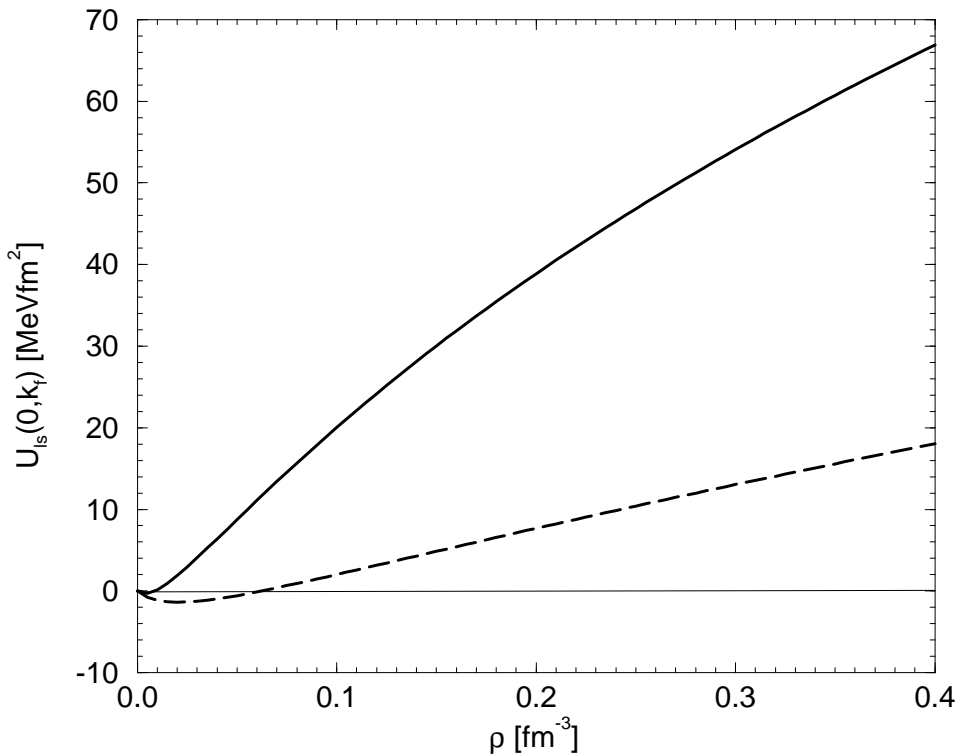


Fig. 6: The full line shows the nuclear spin-orbit strength $U_{ls}(0, k_f)$ at zero nucleon momentum ($p = 0$) versus the nucleon density $\rho = 2k_f^3/3\pi^2$. If the diagrams with two medium insertions are weighted with a factor 1/2 the dashed line results.

In Fig. 7, we show by the full line the dependence of the calculated nuclear spin-orbit strength $U_{ls}(p, k_{f0})$ at saturation density $k_{f0} = 272.7$ MeV on the nucleon momentum p for

$0 \leq p \leq k_{f0}$. One observes a very strong p -dependence which leads even a sign change of $U_{ls}(p, k_{f0})$ above $p = 200$ MeV. Again, this strong p -dependence of $U_{ls}(p, k_{f0})$ has its origin in the alternating signs of the large contributions from individual diagrams as well as their own specific p -dependence. The numerical values in the second and third row of Table 1 indicate how these contributions from individual diagrams change with the nucleon momentum from $p = 0$ to $p = k_{f0}$. One also should keep in mind that the scale relevant for momentum dependences is here set by the pion mass, $m_\pi = 135$ MeV. Note that the ratio p/m_π changes by two units from $p = 0$ to $p = k_{f0}$. Furthermore, the dashed line in Fig. 7 corresponds to the weighting of diagrams with two medium insertions with a factor $1/2$. It shows the same strong p -dependence including a sign change as the full line in Fig. 7.

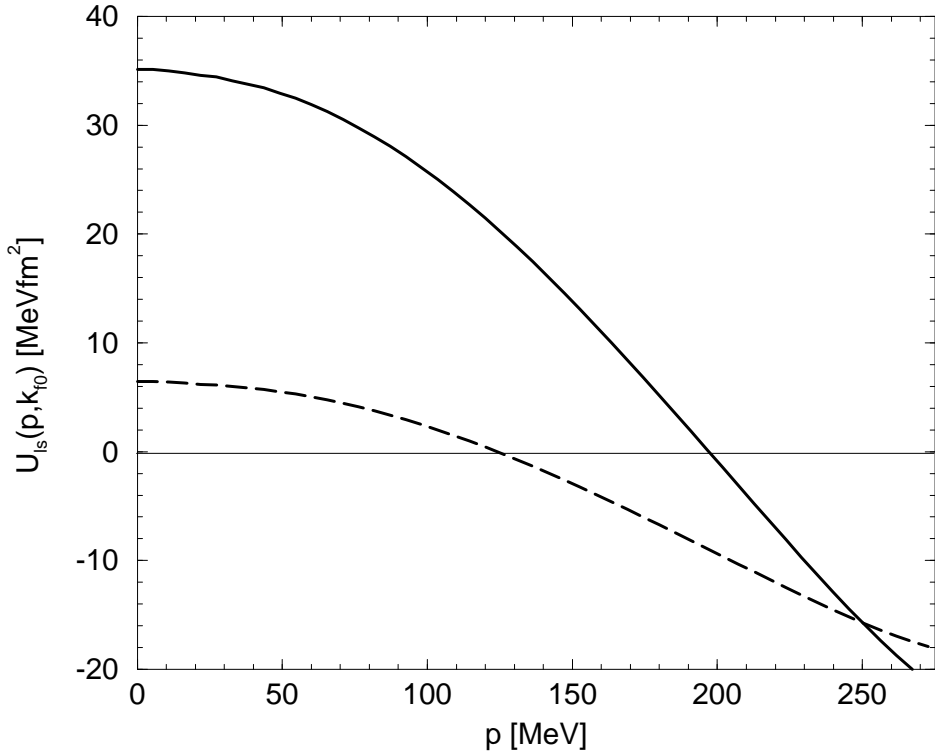


Fig. 7: The momentum dependence of the nuclear spin-orbit strength $U_{ls}(p, k_{f0})$ at saturation density $k_{f0} = 272.7$ MeV. The full (dashed) line corresponds to the weighting of diagrams with two medium insertions with a factor 1 ($1/2$).

Let us briefly summarize our results. We have demonstrated here that the nuclear spin-orbit interaction is not necessarily a relativistic effect. Iterated 1π -exchange (i.e. loosely speaking, the 1π -exchange spin-spin and tensor force in second order) generates large nuclear spin-orbit terms which in fact scale linearly with the nucleon mass M . For weakly inhomogeneous nuclear matter and small nucleon momenta ($p \leq 70$ MeV) the spin-orbit strength from iterated 1π -exchange agrees (at saturation density) well with the empirical shell model value $\tilde{U}_{ls} \simeq 35$ MeV fm 2 . The strong p -dependence of $U_{ls}(p, k_{f0})$ (including a sign change) and the different weighting of $\vec{\nabla}f(r)$ and $f(r)\vec{\nabla}f(r)$ at the nuclear surface leave however questions about the ultimate relevance of this 2π -exchange spin-orbit interaction for real nuclear structure. Nuclear structure calculation which use the calculated spin-orbit strength $U_{ls}(p, k_f)$ as input are necessary in order to clarify the role of the spin-orbit interaction generated by 2π -exchange.

4 Isovector single-particle potential

In this section we generalize our previous calculation [8] of the single-particle potential to isospin asymmetric (homogeneous) nuclear matter. Any relative excess of neutrons over protons in the nuclear medium leads to a different single-particle potential for a proton and a neutron. This fact is expressed by the following decomposition of the single-particle potential in isospin asymmetric nuclear matter:

$$U(p, k_f) + i W(p, k_f) - [U_I(p, k_f) + i W_I(p, k_f)] \tau_3 \delta + \mathcal{O}(\delta^2). \quad (26)$$

Here, $U(p, k_f) + i W(p, k_f)$ is the (complex) single-particle potential in isospin symmetric nuclear matter. The term linear in the isospin asymmetry parameter $\delta = (N - Z)/(N + Z)$ defines the (complex) isovector single-particle potential $U_I(p, k_f) + i W_I(p, k_f)$, and $\tau_3 \rightarrow \pm 1$ for a proton or a neutron. The situation of an isospin asymmetric nuclear medium is realized by the simple substitution:

$$\theta(k_f - |\vec{p}_j|) \rightarrow \frac{1 + \tau_3}{2} \theta(k_p - |\vec{p}_j|) + \frac{1 - \tau_3}{2} \theta(k_n - |\vec{p}_j|), \quad (27)$$

in the medium insertion eq.(4). Here, $k_{p,n} = k_f(1 \mp \delta)^{1/3}$ denote the (different) Fermi momenta of protons and neutrons. Differences in comparison to the calculation of $U(p, k_f) + i W(p, k_f)$ in ref.[8] occur only with respect to isospin factors and the radii of the Fermi-spheres, $k_{p,n} = k_f(1 \mp \delta)^{1/3}$. In practise the isovector single-particle potential $U_I(p, k_f) + i W_I(p, k_f)$ is obtained by differentiating the τ_3 -components of the diagrammatic expressions with respect to δ at $\delta = 0$.

4.1 Real part

Without going into further technical details we enumerate now the individual contributions to the real part of the isovector single-particle potential $U_I(p, k_f)$.

i) 1π -exchange Fock diagram in Fig. 1 including the relativistic $1/M^2$ -correction:

$$U_I^{(1\pi)}(p, k_f) = \frac{g_A^2 m_\pi^3 u^2}{3(4\pi f_\pi)^2} \left\{ 2L(x, u) - 2u + \frac{m_\pi^2}{M^2} \left[u(u^2 + x^2) - (u^2 + x^2)L(x, u) + \frac{u(u^2 - x^2)^2}{2[1 + (u + x)^2][1 + (u - x)^2]} \right] \right\}, \quad (28)$$

with $x = p/m_\pi$ and $u = k_f/m_\pi$. The auxiliary function $L(x, u)$ has been defined in eq.(7).

ii) Iterated 1π -exchange Hartree graphs in Fig. 2:

$$U_I^{(a)}(p, k_f) = \frac{g_A^4 M m_\pi^4 u^2}{48\pi^3 f_\pi^4} \left\{ \left(\frac{u}{x} - 1 \right) \arctan(u - x) - \left(\frac{u}{x} + 1 \right) \arctan(u + x) + \frac{5}{2} L(x, u) \right\}, \quad (29)$$

$$U_I^{(b)}(p, k_f) = \frac{2g_A^4 M m_\pi^4}{3(4\pi f_\pi)^4} \int_{-1}^1 dy \left\{ 2u^2 \ln \frac{u + xy}{u - xy} \left[\frac{2s^2 + s^4}{1 + s^2} - 2 \ln(1 + s^2) \right] - \frac{s^5 s'}{(1 + s^2)^2} \left[2uxy + (u^2 - x^2 y^2) \ln \frac{u + xy}{u - xy} \right] \right\}, \quad (30)$$

with $s' = u \partial s / \partial u$ and the auxiliary function s has been defined after eq.(11).

$$U_I^{(c)}(p, k_f) = \frac{4g_A^4 M m_\pi^4}{3(4\pi f_\pi)^4} \int_{-1}^1 dy \int_{-xy}^{s-xy} d\xi \frac{(xy + \xi)^5}{s[1 + (xy + \xi)^2]^2} \left\{ s'(2\xi + xy) \left[\xi \ln \frac{u + \xi}{u - \xi} - 2u \right] - \frac{2s'}{1 + (xy + \xi)^2} \left[2u\xi + (u^2 - \xi^2) \ln \frac{u + \xi}{u - \xi} \right] - (2s + s') u^2 \ln \frac{u + \xi}{u - \xi} \right\}, \quad (31)$$

$$\begin{aligned}
U_I^{(d)}(p, k_f) = & \frac{4g_A^4 M m_\pi^4}{3(4\pi f_\pi)^4} \int_0^u d\xi \frac{\xi^2}{x} \int_{-1}^1 dy \left\{ \frac{2x\xi y}{x^2 - \xi^2 y^2} \left[\frac{2\sigma^2 + \sigma^4}{1 + \sigma^2} - 2 \ln(1 + \sigma^2) \right] \right. \\
& \left. + \left[\frac{\sigma^2}{(1 + \sigma^2)^2} (5\sigma^4 + 9\sigma^2 + 6 - 4\sigma^3\sigma') - 6 \ln(1 + \sigma^2) \right] \ln \frac{|x + \xi y|}{|x - \xi y|} \right\}, \quad (32)
\end{aligned}$$

with $\sigma' = u \partial\sigma/\partial u$ and the auxiliary function σ has been defined after eq.(15). The symbol $\int_{-1}^1 dy$ stands for a principal value integral.

iii) Iterated 1π -exchange Fock graphs in Fig. 3:

$$\begin{aligned}
U_I^{(e)}(p, k_f) = & \frac{5g_A^4 M m_\pi^4 u^2}{6(4\pi)^3 f_\pi^4} \left\{ -2u + \int_{(u-x)/2}^{(u+x)/2} \frac{d\xi}{x(1 + 2\xi^2)} \right. \\
& \left. \times \left[(1 + 4\xi^2) \arctan 2\xi - (1 + 8\xi^2 + 8\xi^4) \arctan \xi \right] \right\}, \quad (33)
\end{aligned}$$

$$\begin{aligned}
U_I^{(f)}(p, k_f) = & \frac{g_A^4 M m_\pi^4}{3(4\pi f_\pi)^4} \left\{ -\frac{u G(x, u)}{4x^2} \frac{\partial G(x, u)}{\partial u} \right. \\
& \left. + \int_{-1}^1 dy \int_{-1}^1 dz \frac{yz \theta(y^2 + z^2 - 1)}{|yz| \sqrt{y^2 + z^2 - 1}} \frac{s^3 s'}{1 + s^2} [t^2 - \ln(1 + t^2)] \right\}, \quad (34)
\end{aligned}$$

with the auxiliary function $G(x, u) = u(1 + u^2 + x^2) - [1 + (u + x)^2][1 + (u - x)^2] L(x, u)$.

$$\begin{aligned}
U_I^{(g')}(p, k_f) = & \frac{g_A^4 M m_\pi^4}{3(4\pi f_\pi)^4} \left\{ G(u, u) \left[(1 + x^2 - u^2) L(x, u) - u \right] \right. \\
& \left. + 5u \int_0^u d\xi \left[\frac{1}{\xi} (1 + x^2 - \xi^2) L(x, \xi) - 1 \right] \frac{\partial G(\xi, u)}{\partial u} \right\}, \quad (35)
\end{aligned}$$

$$\begin{aligned}
U_I^{(g'')}(p, k_f) = & \frac{g_A^4 M m_\pi^4}{(4\pi f_\pi)^4} \int_0^u d\xi \frac{\xi^2}{3x} \int_{-1}^1 dy \left\{ \left[\frac{\sigma^2}{1 + \sigma^2} (3 + 5\sigma^2 + 8\sigma\sigma') - 3 \ln(1 + \sigma^2) \right] \right. \\
& \times \left[\ln \frac{|x + \xi y|}{|x - \xi y|} + \frac{1}{R} \ln \frac{|xR + (x^2 - \xi^2 - 1)\xi y|}{|xR + (\xi^2 + 1 - x^2)\xi y|} \right] + \xi \left[\ln(1 + \sigma^2) - \sigma^2 \right] \\
& \times \left[\frac{R'}{R^2} \ln \frac{|xR + (x^2 - \xi^2 - 1)\xi y|}{|xR + (\xi^2 + 1 - x^2)\xi y|} + \frac{y(1 - x^2 + 3\xi^2) - xR'}{R[xR + (x^2 - \xi^2 - 1)\xi y]} \right. \\
& \left. + \frac{y(1 - x^2 + 3\xi^2) + xR'}{R[xR + (\xi^2 + 1 - x^2)\xi y]} - \frac{2xy}{x^2 - \xi^2 y^2} \right] \left. \right\}, \quad (36)
\end{aligned}$$

with $R' = \partial R/\partial \xi$ and the auxiliary function R has been defined after eq.(23).

iv) Irreducible 2π -exchange Hartree and Fock graphs:

$$U_I^{(2\pi)}(p, k_f) = \frac{m_\pi^5 u^2}{18x(4\pi f_\pi)^4} \left\{ J\left(\frac{u+x}{2}\right) - J\left(\frac{u-x}{2}\right) \right\}, \quad (37)$$

$$\begin{aligned}
J(\xi) = & 3(1 + 2g_A^2 + 5g_A^4) \ln^2(\xi + \sqrt{1 + \xi^2}) \\
& + 2 \left[5 + 26g_A^2 - 79g_A^4 + 2\xi^2(1 + 10g_A^2 - 59g_A^4) \right] \xi \sqrt{1 + \xi^2} \ln(\xi + \sqrt{1 + \xi^2}) \\
& + (17 + 242g_A^2 - 787g_A^4) \xi^2 - (3 + 14g_A^2 + 15g_A^4) \xi^4 \\
& + \left[60(1 + 6g_A^2 - 15g_A^4) \xi^2 + 4(1 + 10g_A^2 - 59g_A^4) \xi^4 \right] \ln \frac{m_\pi}{2\Lambda}. \quad (38)
\end{aligned}$$

v) Power divergences specific for cut-off regularization:

$$U_I^{(\Lambda)}(p, k_f) = \frac{2\Lambda k_f^3}{3(4\pi f_\pi)^4} \left[26g_A^4 M + 5(3g_A^2 + 1)(1 - g_A^2)\Lambda \right]. \quad (39)$$

The term linear linear in the cut-off Λ stems from iterated 1π -exchange with a contribution of the Hartree diagram (a) and the Fock diagram (e) in the ratio 8 : 5. The term quadratic in the cut-off Λ , on the other hand, originates from irreducible 2π -exchange. Note that the p -independent contribution to $U_I(p, k_f)$ in eq.(39) is just twice its contribution to the asymmetry energy $A(k_f)$ (see eq.(29) in ref.[7]). This relative factor of 2 is typical for a momentum independent NN-contact interaction, to which the power divergences are completely equivalent, as emphasized in ref.[7]. We use consistently the value $\Lambda = 646.3$ MeV $\simeq 7f_\pi$ of the cut-off scale which has been fine-tuned in ref.[7] to the binding energy per particle, $-\bar{E}(k_{f0}) = 15.26$ MeV.

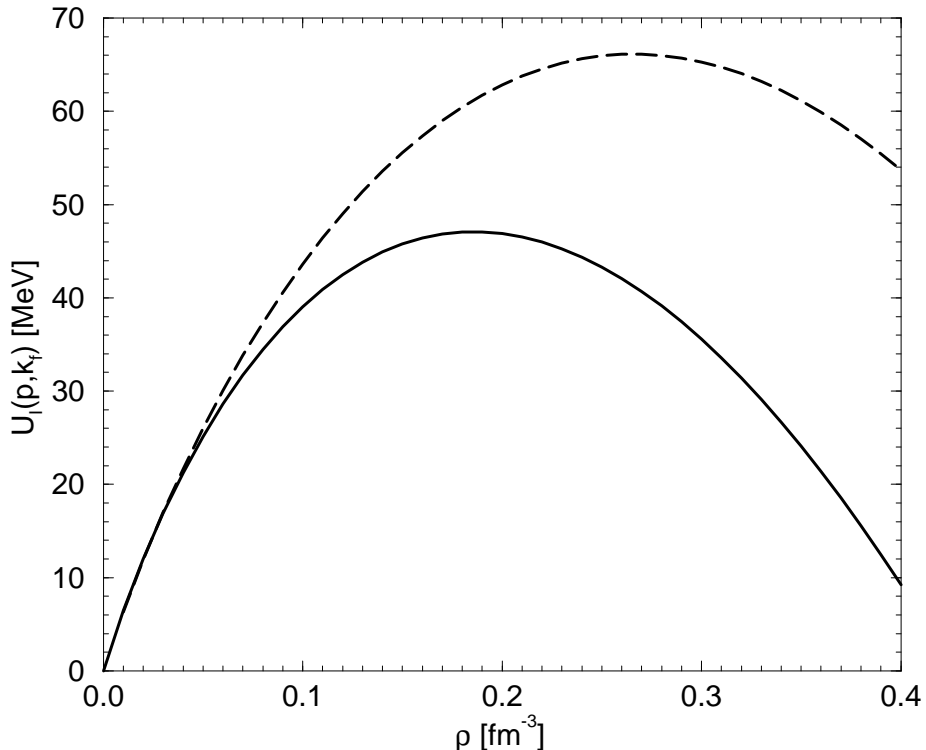


Fig. 8: The real part of the isovector single-particle potential $U_I(p, k_f)$ in isospin asymmetric nuclear matter versus the nucleon density $\rho = 2k_f^3/3\pi^2$. The full (dashed) line corresponds to $p = 0$ ($p = k_f$).

In Fig. 8, we show by the full line the total (real) isovector single particle potential $U_I(0, k_f)$ of our calculation for a nucleon at rest ($p = 0$) as a function of the nucleon density $\rho = 2k_f^3/3\pi^2$. The shape of this curve is very similar to the asymmetry energy $A(k_f)$ (see Fig. 7 in ref.[7]). In comparison to $A(k_f)$ the scale on the ordinate is stretched by a factor of about 1.4. Interestingly, the (real part of the) isovector single-particle potential $U_I(0, k_f)$ has its maximum close to the saturation density $\rho_0 = 0.178$ fm $^{-3}$. The actual value at that point is $U_I(0, k_f) = 47.0$ MeV. This prediction is comparable to the value $U_1 \simeq 33$ MeV [11] used in shell model calculations or the value $U_1 \simeq 40$ MeV [13] deduced from nucleon-nucleus scattering in the framework of the optical model. The dashed line in Fig. 8 shows the density dependence of the (real) isovector single-particle potential $U_I(k_f, k_f)$ at the Fermi surface $p = k_f$. At that point the

(real) isovector single-particle potential comes out always more repulsive than at $p = 0$. Note also that the (possibly unrealistic) downward bending branches of the curves in Fig. 8 start at densities higher than those relevant for conventional nuclear physics.

Furthermore, we show in Fig. 9 the momentum dependence of the (real) isovector single-particle potential $U_I(p, k_{f0})$ at saturation density $k_{f0} = 272.7$ MeV. The p -dependence of $U_I(p, k_{f0})$ is non-monotonic in the interval $0 \leq p \leq k_{f0}$. One observes a broad maximum at $p = 230$ MeV where $U_I(p, k_{f0})$ has increased by about 30% to the value 62.9 MeV. Note that in comparison to the spin-orbit strength $U_{ls}(p, k_{f0})$ shown in Fig. 7 the p -dependence of the real part of the isovector single-particle potential $U_I(p, k_{f0})$ is very moderate. Most useful would be nuclear structure calculations using the calculated isovector single particle potential $U_I(p, k_f)$ as input.

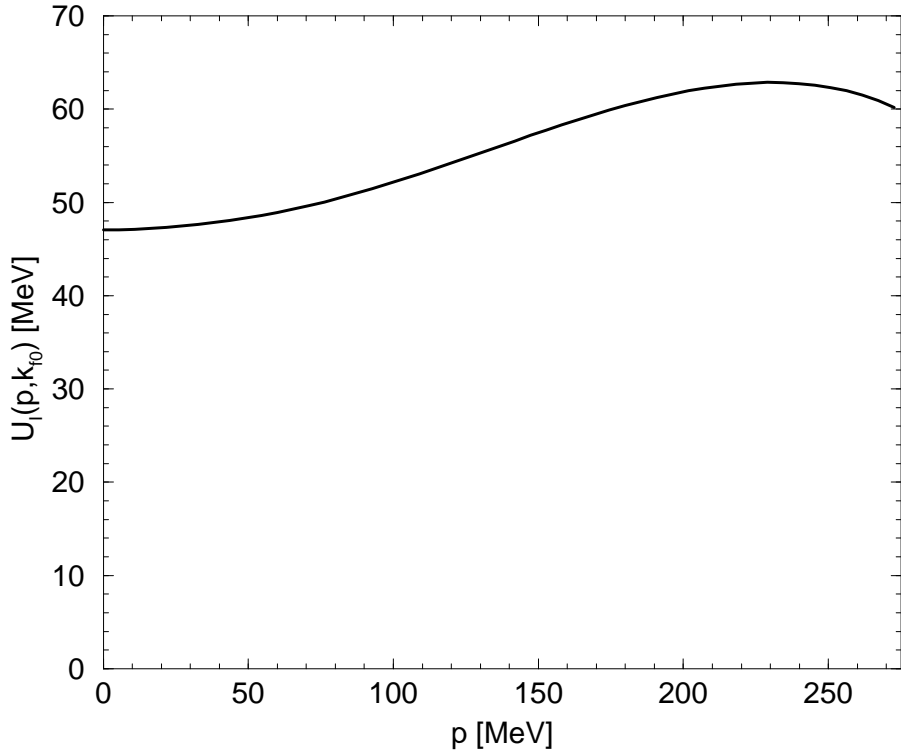


Fig. 9: The momentum dependence of the real part of the isovector single-particle potential $U_I(p, k_{f0})$ at saturation density $k_{f0} = 272.7$ MeV.

4.2 Imaginary part

In this subsection, we discuss the imaginary part $W_I(p, k_f)$ of the isovector single-particle potential. According to eq.(26), it splits and shifts the half-width of a neutron-hole state and a proton-hole state in the Fermi-sea (with momentum $0 \leq p \leq k_f$) by the amount $\pm \delta W_I(p, k_f)$. Within the present calculation the imaginary part $W_I(p, k_f)$ arises entirely from iterated one-pion exchange. It is advantageous to present analytical formulas only for complete classes of diagrams. We find from the iterated 1π -exchange Hartree diagrams in Fig. 2 (including the analogous graph with three medium insertions) the following contribution to the imaginary isovector single-particle potential:

$$W_I^{(H)}(p, k_f) = \frac{g_A^4 M m_\pi^4}{192\pi^3 f_\pi^4} \left\{ 2u^4 - 10u^2 - \frac{14}{3}u^2 x^2 + 8u^2 \ln(1 + 4x^2) \right\}$$

$$\begin{aligned}
& + \frac{5u^2}{x} \left[\arctan(u-x) - \arctan(u+x) + 2 \arctan 2x \right] \\
& - 2u^2 \left(1 + \frac{u}{x} \right) \ln[1 + (u+x)^2] + 2u^2 \left(\frac{u}{x} - 1 \right) \ln[1 + (u-x)^2] \\
& + \int_{-1}^1 dy \left\{ 2u^2 \left[\frac{2s^2 + s^4}{1 + s^2} - 2 \ln(1 + s^2) \right] + \frac{(x^2 - u^2)s^5 s'}{2(1 + s^2)^2} \right. \\
& + \int_0^u d\xi \xi^2 \left[\delta(x - \xi|y|) \left(2 \ln(1 + \sigma^2) - \frac{2\sigma^2 + \sigma^4}{1 + \sigma^2} \right) + \theta(x - \xi|y|) \right. \\
& \left. \left. \times \frac{1}{x} \left(\frac{\sigma^2}{1 + \sigma^2} (6 + 9\sigma^2 + 5\sigma^4 - 4\sigma^3\sigma') - 6 \ln(1 + \sigma^2) \right) \right] \right\}. \quad (40)
\end{aligned}$$

The iterated 1π -exchange Fock diagrams in Fig. 3 (again including the analogous graph with three medium insertions) lead, on the other hand, to the following expression:

$$\begin{aligned}
W_I^{(F)}(p, k_f) = & \frac{\pi g_A^4 M m_\pi^4}{3(4\pi f_\pi)^4} \left\{ u^2 \ln(1 + 4x^2) + \frac{u^2}{x} \arctan 2x - u^2(2 + 5u^2 + 3x^2) \right. \\
& + \int_0^1 dz \frac{u^2 [4x^2 z^2 - \ln(1 + 4x^2 z^2)]}{\sqrt{(1 + x^2 - u^2)^2 + 4(u^2 - x^2 z^2)}} + \frac{5u^2}{x} \int_{(u-x)/2}^{(u+x)/2} d\xi \frac{1 + 4\xi^2}{1 + 2\xi^2} \\
& \times \ln(1 + 4\xi^2) + \int_{-1}^1 dy \left\{ \int_{-1}^1 dz \frac{\theta(1 - y^2 - z^2)}{\pi \sqrt{1 - y^2 - z^2}} \frac{s^3 s'}{1 + s^2} [t^2 - \ln(1 + t^2)] \right. \\
& + \int_0^u d\xi \frac{\xi^2}{x} \left[\theta(x - \xi|y|) \frac{\xi R'}{R^2} (\sigma^2 - \ln(1 + \sigma^2)) + \left(1 - \frac{1}{R} \right) [\theta(x - \xi|y|) \right. \\
& \times \left. \left(\frac{\sigma^2}{1 + \sigma^2} [\sigma\sigma' [8 - 10\theta(\xi - x)] + 3 + 5\sigma^2] - 3 \ln(1 + \sigma^2) \right) \right. \\
& \left. \left. + x \delta(x - \xi|y|) (\ln(1 + \sigma^2) - \sigma^2) - \frac{2u^2 \sigma_x^3 \theta(x - \xi)}{(\sigma_x - \xi y)(1 + \sigma_x^2)} \right] \right\}, \quad (41)
\end{aligned}$$

with the auxiliary function $\sigma_x = \xi y + \sqrt{u^2 - x^2 + \xi^2 y^2}$. If the delta-function $\delta(x - \xi|y|)$ is used to eliminate the dy -integration in eqs.(40,41) the remaining $d\xi$ -integral extends over the restricted region $x \leq \xi \leq u$. The sum of both contributions eqs.(40,41) evaluated at zero nucleon momentum ($p = 0$) can even be written as a closed form expression:

$$W_I(0, k_f) = \frac{g_A^4 M m_\pi^4 u^2}{384\pi^3 f_\pi^4} \left\{ \frac{9u^6 + 40u^4 + 27u^2}{2(1 + u^2)^2} - \frac{12u^4 + 40u^2 + 27}{(1 + u^2)(2 + u^2)} \ln(1 + u^2) \right\}. \quad (42)$$

Finally, we show in Fig. 10 the momentum dependence of the imaginary isovector single-particle potential $W_I(p, k_{f0})$ at saturation density $k_{f0} = 272.7$ MeV. The associated value at zero nucleon momentum, $W_I(0, k_{f0}) = 26.7$ MeV, agrees within 10% with the isoscalar half-width $W(0, k_{f0}) = 29.7$ MeV found in ref.[8]. As a consequence of the decreasing phase space available for redistribution of a nucleon-hole state's energy, the curve in Fig. 10 drops with momentum p and $W_I(p, k_{f0})$ reaches zero at the Fermi-surface $p = k_{f0}$. The exact vanishing of $W_I(p, k_f)$ at the Fermi-surface $p = k_f$ is even separately true for the class of iterated 1π -exchange Hartree diagrams and the class of iterated 1π -exchange Fock diagrams. The conditions $W_I^{(H)}(k_f, k_f) = 0$ and $W_I^{(F)}(k_f, k_f) = 0$ serve as an excellent (analytical and numerical) check on the involved calculations leading to eqs.(40,41).

In summary, we find that the predictions from chiral 1π - and 2π -exchange for the real part of the isovector single-particle potential $U_I(p, k_f)$ agree fairly well with empirical values. The calculated imaginary part $W_I(p, k_f)$ fulfills the constraints imposed by Luttinger's theorem [14].

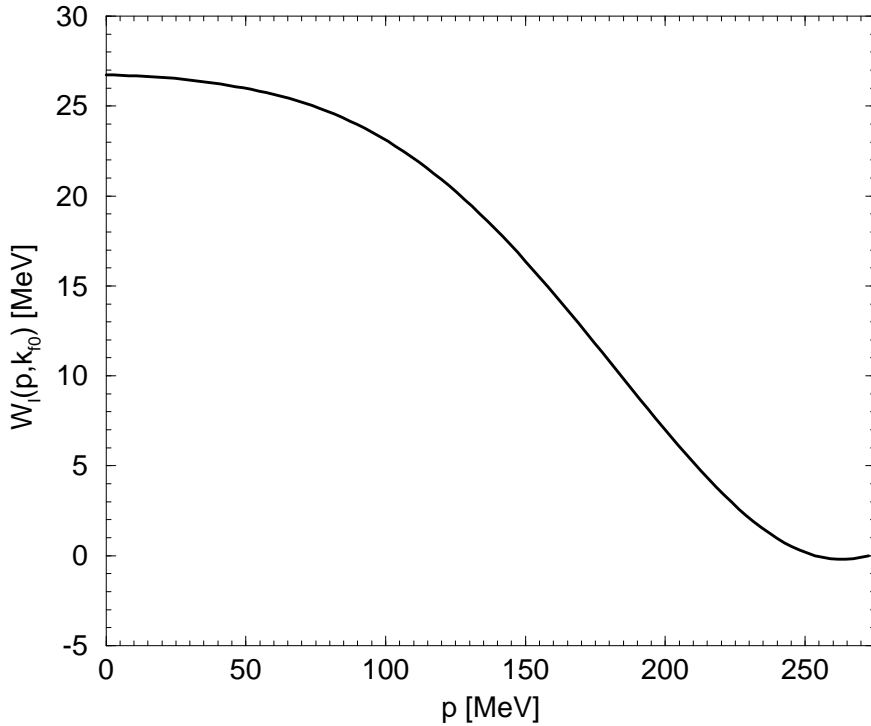


Fig. 10: The momentum dependence of the imaginary part of the isovector single-particle potential $W_I(p, k_{f0})$ at saturation density $k_{f0} = 272.7$ MeV.

References

- [1] O. Haxel, J.H.D. Jensen and H.E. Suess, *Phys. Rev.* **75** (1949) 1766; M. Goeppert-Mayer, *Phys. Rev.* **75** (1949) 1969.
- [2] B.D. Serot and J.D. Walecka, *Adv. Nucl. Phys.* **16** (1986) 1; and refs. therein.
- [3] P. Ring, *Prog. Part. Nucl. Phys.* **37** (1996) 193; and refs. therein.
- [4] S. Typel and H.H. Wolter, *Nucl. Phys.* **A656** (1999) 331; and refs. therein.
- [5] F. Hofmann, C.M. Keil and H. Lenske, *Phys. Rev.* **C64** (2001) 034314; and refs. therein.
- [6] N. Kaiser, R. Brockmann and W. Weise, *Nucl. Phys.* **A625** (1997) 758.
- [7] N. Kaiser, S. Fritsch and W. Weise, *Nucl. Phys.* **A697** (2001) 255. For an earlier similar approach see: M. Lutz, B. Friman and C. Appel, *Phys. Lett.* **B474** (2000) 7.
- [8] N. Kaiser, S. Fritsch and W. Weise, *Nucl. Phys.* **A700** (2001) 343.
- [9] S. Fritsch, N. Kaiser and W. Weise, nucl-th/0202005, submitted to *Phys. Lett.* **B**.
- [10] R. Brockmann and R. Machleidt, *Phys. Rev.* **C42** (1990) 1965.
- [11] A. Bohr and B.R. Mottelson, Nuclear Structure, Vol.I, Benjamin, (1969), chapt. 2.4.
- [12] G. Eder, Kernmaterie, Spektrum Akademischer Verlag, (1995), chapt. 4.1.
- [13] P.E. Hodgson, Growth Points in Nuclear Physics, Vol. 3, Pergamon Press, (1981), chapt. 2.
- [14] J.M. Luttinger, *Phys. Rev.* **121** (1961) 942.
- [15] R.M. Dreizler and E.K.U. Gross, Density Functional Theory, Springer Verlag, (1990), chapt. 5.
- [16] L. Münchow and R. Reif, Recent Developments in the Nuclear Many-Body Problem, Vol. 1, Teubner Verlagsgesellschaft, Leipzig, (1985), chapt. 4.6.
- [17] S.C. Pieper, V.R. Pandharipande, R.B. Wiringa and J. Carlson, *Phys. Rev.* **C64** (2001) 014001.